Journal of Iraqi Al-Khwarizmi (JIKh) Volume:10 Issue: 2 Year: 2026 pages: 587- 595

A Posteriori Estimator for 1D WG Transport

Authors Names

Hayder Ismael Neamah[a]

Publication date: 29 /10 /2026

Keywords: weak Galerkin method; transport-reaction equation; a posteriori error estimation; characteristic reconstruction; residual lifting; error identity..

ABSTRACT

This paper develops a full computable a posteriori estimator for a one-dimensional stationary transport reaction equation discretized by a global stabilization weak Galerkin method. While a continuous piecewise linear reconstruction is organized from the nodal element, the cell and nodal unknowns of the distinct solution are retained. The reconstruction rest is raised along the transport feature. In one space dimension, the raised rest is just the reconstruction mistake; accordingly, its transport energy provides an exact a posteriori identity and a crisp estimator with unit effectiveness up to numerical quadrature. A coarse residual norm upper edge and a computable cell-to-reconstruction disagreement give a guaranteed edge for the WG cell variable. Local shares of the upraised energy thrust a Dörfler-marked adaptive loop, and two smooth constructed instances affirm second order decay and unit effectiveness, while a sharp-front instance demonstrates that 19 adaptively selected elements cut the reconstruction mistake to $1.881\times10^{-}3$, compared with $1.261\times10^{-}2$ on a uniform mesh of the identical size. Wall time measuring's quantify the additional cost of residual raising, and the share is an error-certification and adaptive-control mechanism for a generic WG discretization instead than a novel inflated strategy.

1. Introduction

Weak Galerkin (WG) methods stand for a distinct function by independent inside and boundary elements and replace classical differentials by weakly specified distinct operators. Since backed up a wide household of nonconforming discretizations, the building was presented for elliptic issues by Wang and Ye [1] and has. Residual a posteriori studies for elliptic WG strategies sets up that the additional boundary unknowns can be integrated into dependable and efficient estimators [2,3]. Subsequent, various boundary conditions were handled, modified preparations, and polygonal meshes [4,5].

For first order inflated equations, stability depends on way, influx data, and the sign of the boundary flux. Zhang and Zhang developed stable WG preparations for stationary and time-dependent symmetrical inflated systems and turned out a priori convergence approximations [6,7]. Upwind and WENO discrepancies farther showed the flexibility of the WG model for transport equations [8], a lower-order preparation and depicted energy stability and numerical convergence [9]. These contributions concern the design and a priori analysis of the discretization; they do not by themselves supply the reconstruction-based a posteriori identity turned out below.

A posteriori analysis for convection-dominated problems is delicate given that an energy norm only may not capture all footings brought forth by residual location. While Ern, Stephansen, and Vohralik developed guaranteed flux-reconstruction bounds for discontinuous Galerkin convection-diffusion-reaction estimates [11], sharma obtained robust upper and low bounds for a convection-diffusion WG method [10],. The general differentiation between a computable upper bound, an efficient index, and an exact mistake identity is stressed in the review by Chamoin and Legoll [12].The present work takes a purposely curtailed path. Rather than presuming a multidimensional lifting approximation, it applies

[a]*Department of Mathematics, faculty of education, University of Al-Qadisiyah, 58002 Al-Qadisiyah, Iraq., E-Mail: hayder.neamah@edu.qu..iq*

the characteristic construction of a scalar one-dimensional transport operator, and this takes to a residual-lift issue whose solution equals the reconstruction error. The result is crisp and full computable, however it evidences the reconstructed solution; the WG cell variable is then controlled by adding a computable disagreement. This separation makes each analytic measure visible and prevents numerical understanding from being replaced for a missing theorem. Takes a purposely curtailed path. Rather than presuming a multidimensional lifting approximation, it applies the characteristic construction of a scalar one-dimensional transport operator. This takes to a residual-lift issue whose solution equals the reconstruction error. The result is crisp and full computable, however it evidences the reconstructed solution; the WG cell variable is then controlled by adding a computable disagreement. This separation makes each analytic measure visible and prevents numerical understanding from being replaced for a missing theorem.

2. Model problem and weak Galerkin discretization

2.1 Continuous problem

Let I = (0, 1), let a > 0 and b ≥ b0 > 0 be constants, and see

$$au' + bu = f \text{ in I}, \quad u(0) = u_{in} \tag{2.1}$$

For f ∈ L^2(I) and dictated inflow value u_{in}, the issue has a unparalleled solution in the transport graph space $\mathbf{X} = \{\mathbf{v} \in \mathbf{L^{2(I)}}: \mathbf{v'} \in \mathbf{L^{2(I)}}\} = \mathbf{H^{1(I)}}$. The equality with H^1 is specific to one dimension and is just the property that neglects for an individual directional differential in several dimensions.

2.2 Discrete space and weak derivative

Let T_h be a partition with elements K= (x_i, xi_{+1}). For polynomial degree k ≥1, a WG function is v_h= {v_0, v_b}, where v_0| K ∈ P_k(K) and v_b is single-valued at each mesh node. For q ∈ P_k(K), the weak transport derivative is defined by

$$(D_w^a v_h, q)_K = -(a\, v_0, q')_K + \langle a\, n_K v_b, q \rangle_{\partial K} \tag{2.2}$$

With the scalar boundary matrix M=a and a global parameter μ>a/2, define

$$A_{h(w_h,v_h)} = (D_w^a w_h, v_0)_{\{\mathcal{T}_h\}} + (b\, w_0, v_0)_{\{\mathcal{T}_h\}} + \mu\langle w_0 - w_b, v_0 - v_b\rangle_{\{\partial\mathcal{T}_h\}} + \frac{1}{2}\langle (M - a\, n) w_b, v_b\rangle_{\{\partial I\}} \tag{2.3}$$

The WG solution u_h satisfies

$$A_{h(u_h,v_h)} = (f, v0)_{Th} + ½\langle g, vb\rangle \partial I \ \ for\ all\ v_h, \tag{2.4}$$

Where g = (M − an)u on the boundary. Since a >0 and M=a, only the inflow value contributes to the right-hand side.

2.3 Discrete energy identity

Testing the weak derivative with v_b and summing the two endpoint contributions gives

$$A_{h(v_h,v_h)} = b\|v_0\|^2 + \Sigma K\langle(\mu - \tfrac{1}{2}an_K)(v_0 - v_b)^2, 1\rangle\,\partial K + \tfrac{1}{2}a[v_b(0)^2 + v_b(1)^2]. \qquad (2.5)$$

Given that $\mu > a/2$, each term on the accurate is nonnegative and the ensuing distinct issue is coercive. Equation (2.5) is applied to verify the implementation; the a posteriori evidence below applies the continuous transport stability of the reconstruction instead than deriving a continuous mistake approximation from distinct coercivity.

3. Reconstruction and computable estimators

3.1 Continuous reconstruction

For the P_1 implementation, define $C_h u_h$ as the continuous piecewise-linear function whose nodal values are the WG face values:

$$(C_h u_h)(x_i) = u_b(x_i), \qquad (C_h u_h) \mid K \in P_1(K). \qquad (3.1)$$

Write $w_h = C_h u_h$. Its strong residual and inflow mismatch are

$$r_h = f - aw_h' - bw_h, \qquad \delta_h = u_{in} - w_h\,(0). \qquad (3.2)$$

3.2 Characteristic residual lift

As the solution of the computable residual-lift issue, define z_h:

$$az_h' + bz_h = r_h \ \text{in I}, \qquad z_h(0) = \delta_h. \qquad (3.3)$$

The lift can be assessed by elementwise characteristic integrating or by a high-order one-dimensional ODE solver, and it applies just the known data and the computed reconstruction.

Theorem 3.1

Let u solve (2.1), let u_h solve (2.4), and let w_h and z_h be defined by (3.1)-(3.3). Then $z_h = u - w_h$ and

$$\eta_{char}^2 := b\|z_h\|_{L^2}^2\ (I) + a|z_h(1)|^2 = b\|u - w_h\|_{L^2}^2\ (I) + a|u(1) - w_h(1)|^2. \qquad (3.4)$$

Deducting the equation for w_h from (2.1) demonstrates that $e = u - w_h$ lives up to $ae' + be = r_h$ and $e(0) = \delta_h$, and the first-order initial-value issue has a unparalleled H^1 solution, therefore $e = z_h$. Substitution provides (3.4). No unknown multiplicative constant or unproved regularity premise comes in the identity.

Corollary 3.2

Multiplying (3.3) by z_h, integrating by parts, and applying Young's inequality supplies

$$\eta_{char}^2 \le b^{-1}\|r_h\|_{L^2}^2(I) + a|\delta_h|^2 =: \eta_{res}^2. \qquad (3.5)$$

The edge η_{res} is cheap and guaranteed, however it demand not be efficient given that it disregards cancellation of the residual along features. The numerical section studies it just to show this differentiation.

Corollary 3.3

Allow $d_h = \|w_h - u_0, h\|L^2(I)$, which is full computable, and the triangle inequality and (3.4) output

$$\|u - u_0, h\|L^2(I) \leq b^{\frac{-1}{2}}\eta_{char} + d_h \qquad (3.6)$$

Therefore the exact reconstruction estimator and the cell-to-reconstruction disagreement jointly evidences the cell element, and this statement does not claim an exact identity for u_0, h itself.

3.3 Local contributions and adaptive marking

For each element K, define the local lifted-energy contribution

$$\eta_k^2 = \mathrm{b}\|\mathrm{z_h}\|_{\mathrm{L^2}}^2(\mathrm{K}) + 1_{\{\mathrm{K}=\mathrm{K_{out}}\}}\ \mathrm{a}|\mathrm{z_h}(1)|^2, \qquad \eta_{\mathrm{char}}^2 = \Sigma_{\mathrm{K}}\,\eta_k^2 \qquad (3.7)$$

Given a marking parameter 0< θ <1, a minimal set M_h is selected so that

$$\Sigma_{\{K\in M_h\}}\,\eta_K^2 \geq \theta\,\Sigma_K\,\eta_K^2 \qquad (3.8)$$

The pronounced intervals are bisected and the sequence solve-reconstruct-lift-mark-refine is reiterated, and equation (3.7) is an exact decomposition of the certified reconstruction amount. It is not, by itself, an evidence of optimum adaptive complexity; the adaptive comparison is therefore regarded as numerical evidence.

4. Numerical methodology

The experimentations apply a=1.3, b=1, μ=2, M=a, and P_1 cell polynomials with one face value at each node. Component integrals are assessed by 12-point Gauss-Legendre quadrature, and the residual-lift equation is incorporated by fourth-order Runge-Kutta with 80 substeps per component. The assembled WG linear systems are figured out in twofold precision; the displayed reconstruction is calculated from the ensuing face unknowns and is not made by troubling the analytic solution. The two smooth trials apply uniform meshes. The adaptive trial begins from eight intervals, usages θ=0.55, and bisects taged intervals. Four amounts are monitored: the reconstruction energy in (3.4), η_{char} the coarse edge η_{res}, and the algebraic infinity-norm residual. Effectivity is specified as η_{char} separated by the reconstruction energy. The WG projection mistake and the cell-to-reconstruction disagreement are too calculated however are not replaced for the certified reconstruction mistake.

5. Numerical results

5.1 Example 1:

Select u(x) = sin(πx), therefore that f=aπcos(πx)+bsin(πx) and u_{in} = 0. Table 1 demonstrates second-order decay of the continuous reconstruction error. While the algebraic residual remains near machine precision, the characteristic estimator concurs with the mistake to six described decimal spots. Figure 2

overlays the analytic solution and the independently calculated N=64 reconstruction; its low panel exhibits the pointwise absolute mistake. While a second surface presents the absolute mistake and its reduction under polish, figure 3 shows a third-dimensional comparison over place and mesh degree: the analytic wireframe is superposed on the WG reconstruction surface.

Table 1. Smooth-sine reconstruction error and estimator.

N	Error	Rate	η_{char}	Effectivity	Alg. residual
8	4.263822e-03	-	4.263822e-03	1.000000	8.9e-16
16	1.029666e-03	2.050	1.029666e-03	1.000000	4.0e-16
32	2.548819e-04	2.014	2.548820e-04	1.000000	7.1e-16
64	6.355447e-05	2.004	6.355448e-05	1.000000	8.0e-16

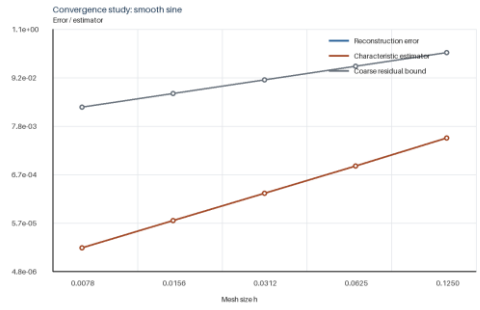


Figure 1. Error, characteristic estimator, and coarse residual bound for the smooth-sine test.

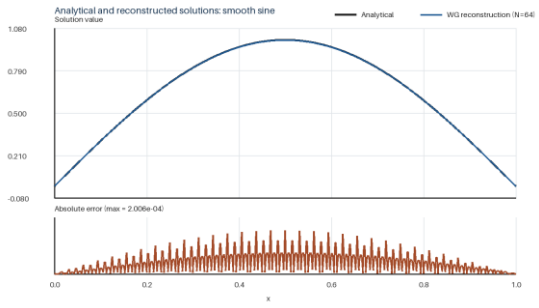


Figure 2. Analytical solution, WG reconstruction on N=64, and pointwise absolute error for the smooth-sine test.

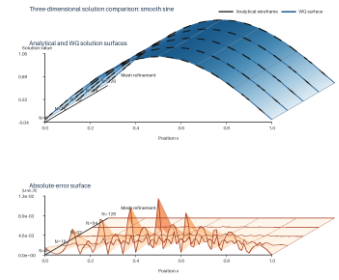


Figure 3. Three-dimensional analytical wireframe, WG reconstruction surface, and absolute-error surface over the five mesh levels.

5.1 Example 2:

Select $u(x) = \exp(x)$, $f = (a + b)\exp(x)$, and $u_{in} = 1$, and this instance verifies the boundary-data term in (3.2)-(3.5). The identical second-order reconstruction trend is found, and the effectiveness stays one within the integrating tolerance. Figs 5 and 6 supply the direct analytical-versus-reconstructed comparison and the corresponding third-dimensional solution and mistake surfaces.

Table 2. Nonzero-inflow reconstruction error and estimator.

N	Error	Rate	η_{char}	Effectivity	Alg. residual
8	1.230225e-03	-	1.230225e-03	1.000000	9.4e-16
16	2.855611e-04	2.107	2.855612e-04	1.000000	1.8e-15
32	6.833722e-05	2.063	6.833722e-05	1.000000	1.9e-15
64	1.668106e-05	2.034	1.668106e-05	1.000000	2.7e-15
128	4.118404e-06	2.018	4.118404e-06	1.000000	2.7e-15

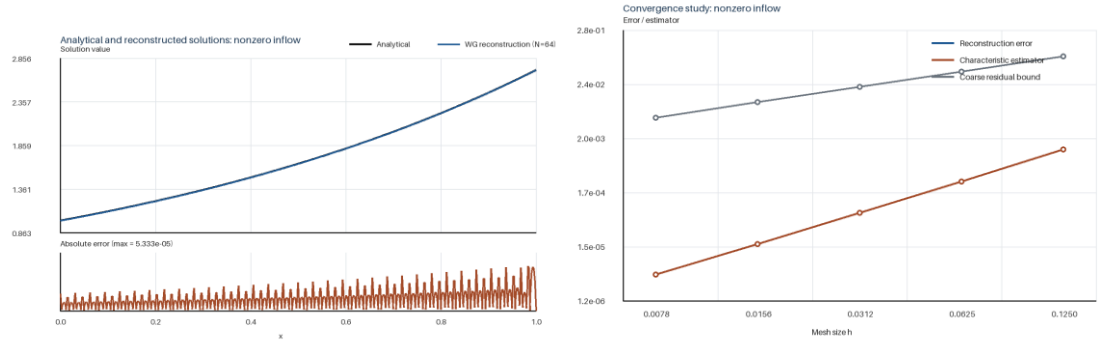


Figure 4. Error, characteristic estimator, and coarse residual bound for the nonzero-inflow test. Figure 5. Analytical solution, WG reconstruction on N=64, and pointwise absolute error for the nonzero-inflow test.

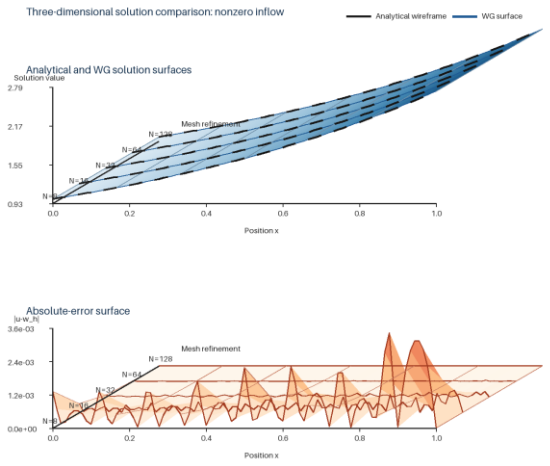


Figure 6. Three-dimensional analytical wireframe, WG reconstruction surface, and absolute-error surface over the five mesh levels.

5.3 Adaptive sharp-front example

To try location instead than asymptotic smooth convergence, select u(x) = ½[1+ tanh((x−0.72)/0.035)] and industry $au' + bu = f$, and the narrow passage is not adjusted purposely with each uniform mesh. Begining from eight elements, the local amounts η_K^2 in (3.7) are taged with θ = 0.55 and The

chosen intervals are bisected. Table 3 compares the adaptive mistake with a uniform WG calculation applying the identical figure of elements.

Table 3. Adaptive sharp-front reconstruction and equal-size uniform comparison.

Cycle	Elements	min h	Adaptive error	Uniform error	Effectivity
0	8	0.1250	6.617467e-02	6.617467e-02	1.000000
1	9	0.0625	1.498616e-02	2.482550e-02	1.000000
2	11	0.0312	9.333745e-03	5.803126e-02	1.000000
3	13	0.0312	7.033936e-03	2.487780e-02	1.000000
4	15	0.0156	6.849975e-03	2.773844e-02	1.000000
5	16	0.0156	3.289327e-03	9.814199e-03	1.000000
6	19	0.0078	1.881352e-03	1.261440e-02	1.000000

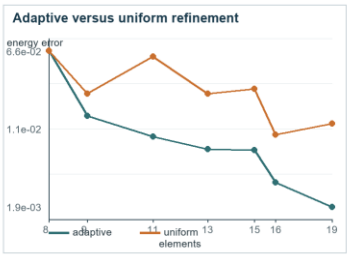
Subsequent to six polishes, the adaptive mesh comprises 19 elements and arrives at an energy mistake of $1.881\times10^{-}3$; the equal-size uniform mesh provides $1.261\times10^{-}2$. Therefore the adaptive mistake is regarding 6.7 times smaller in this trial. The equal-size uniform meshes at sequential adaptive rounds are not a nested polish sequence, and their mistake oscillations reflect the altering coalition of the crisp front with the grid. The small adaptive interval is 0.0078125 and the local distribution concentrates around the passage at x=0.72, and the effectiveness stays within $2.4\times10^{-}7$ of one throughout the loop.

5.4 Measured estimator cost

Table 4 studies the median wall-clock times over five tallies of the present dense-Python implementation, and the comparison divides the WG assembly and linear solution from the Runge-Kutta characteristic lift. These measuring's supply reproducible timing information and quantify the practical computational operating cost of the different elements. They should not, however, be construed as implementation-independent complexity approximations.

Table 4. Prototype wall-time comparison for the smooth-sine test.

Elements	WG solve (s)	Lift (s)	Lift / solve
16	0.0134	0.0545	4.08
32	0.0252	0.1064	4.23
64	0.0512	0.2161	4.22
128	0.1029	0.4292	4.17



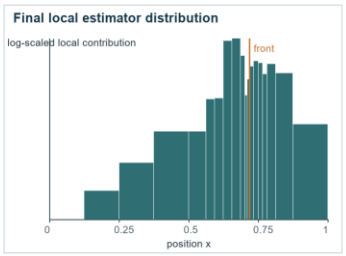


Figure 7. Adaptive-versus-uniform error and final local estimator distribution.

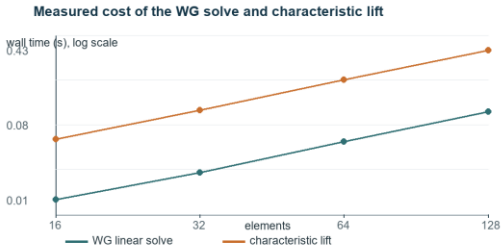


Figure 8. Measured wall time of the WG solve and characteristic lift.

With 80 Runge-Kutta substeps per component, the lift costs more or less four times the WG assembly-and-solve phase over N=16-128, and this is the cost of the near-exact identity. The low-cost residual estimator η_{res} stays beneficial when certification truth is less critical, while the lift can be calculated efficiently applying a closed-form characteristic look or vectorized quadrature.

6. Scope, novelty, and limitations of the study

The distinct WG strategy is inherited from The established weak derivative and stabilization framework [6,7]; the paper does not claim a novel discretization. The share is the usage of a continuous nodal reconstruction together with a characteristic residual lift that brings forth an exact and computable one-dimensional mistake identity. This differs from elliptic WG estimators established on Helmholtz decomposition [2-5] and from convection-diffusion approximations in which diffusion supplies additional regularity [10,11]. The limitation to one dimension is indispensable. In several dimensions, the graph norm commands $a\cdot\nabla v$ however not differentials transverse to a, and standard isotropic projection approximations therefore need an additional adjoint-regularity theorem or an anisotropic reconstruction. The present analysis does not claim reliability for matrix-valued systems, characteristic bounders, k=0 volume-only rests, or optimum adaptive convergence. The adaptive experimentation shows beneficial location however does not turn out contraction or rate optimality. Existing planar calculations in the research archive remain implementation diagnostics and are deliberately omitted from the theorem and publication claims.

7. Conclusions

A full computable a posteriori certification process has been seted up for a one-dimensional scalar WG transport discretization. The face unknowns define a continuous reconstruction; the rest is raised along the transport way; and singularity of the transport initial-value issue turns that lift into the exact reconstruction error. While a simple residual norm provides a cheap however less efficient upper bound, the ensuing estimator has unit theoretical effectiveness. A computable reconstruction disagreement broadens the approximation to the WG cell variable. The local decomposition supports Dörfler mark: in the sharp-front experimentation, 19 adaptive elements cut the mistake by a factor of regarding 6.7 relative to an equal-size uniform locks. The reported timings too create explicit that the near-exact lift is more expensive than the coarse residual edge in the current image.

The next analytic measure is a multidimensional streamline reconstruction with an explicitly turned out transverse-control mechanism. Up to such a result is available, the one-dimensional theorem should be handled as the strict nucleus and the higher-dimensional computations as exploratory grounds.

References

[1] J. Wang and X. Ye, A weak Galerkin finite element method for second-order elliptic problems, Journal of Computational and Applied Mathematics 241 (2013) 103-115.
[2] L. Chen, J. Wang, and X. Ye, A posteriori error estimates for weak Galerkin finite element methods for second order elliptic problems, Journal of Scientific Computing 59 (2014) 496-511.
[3] H. Li, L. Mu, and X. Ye, A posteriori error estimates for the weak Galerkin finite element methods on polytopal meshes, Communications in Computational Physics 26 (2019) 558-578.

[4] S. Xie, M. Han, and P. Zhu, A posteriori error estimate of weak Galerkin FEM for second order elliptic problem with mixed boundary condition, Discrete and Continuous Dynamical Systems - B 26 (2021) 5217-
[5] Y. Zeng, F. Wang, Z. Weng, and H. Hu, A posteriori error estimates for a modified weak Galerkin finite element approximation of second order elliptic problems with DG norm, Journal of Computational Mathematics 39 (2021) 755-776.
[6] T. Zhang and S. Zhang, The weak Galerkin finite element method for the symmetric hyperbolic systems, Journal of Computational and Applied Mathematics 365 (2020) 112375.
[7] T. Zhang and S. Zhang, An explicit weak Galerkin method for solving the first order hyperbolic systems, Journal of Computational and Applied Mathematics 412 (2022) 114311.
[8] L. Mu and Z. Chen, A new WENO weak Galerkin finite element method for time dependent hyperbolic equations, Applied Numerical Mathematics 159 (2021) 106-124.
[9] H. I. Neamah, An upwind finite element method for solving hyperbolic equations, International Journal of Mathematics and Computer Science 20 (2025) 969-977.
[10] N. Sharma, Robust a-posteriori error estimates for weak Galerkin method for the convection-diffusion problem, Applied Numerical Mathematics 170 (2021) 384-397.
[11] A. Ern, A. F. Stephansen, and M. Vohralik, Guaranteed and robust discontinuous Galerkin a posteriori error estimates for convection-diffusion-reaction problems, Journal of Computational and Applied Mathematics 234 (2010) 114-130.
[12] L. Chamoin and F. Legoll, An introductory review on a posteriori error estimation in finite element computations, SIAM Review 65 (2023) 963-1028. https://doi.org/10.1137/21M1464841.